Dynamics of Single Pt Atoms on Alumina during CO Oxidation Monitored by Operando X-ray and Infrared Spectroscopies

C. Dessal, T. Len, F. Morfin, J. Rousset, M. Aouine, P. Afanasiev, L. Piccolo

Dynamics of single Pt atoms on alumina during CO oxidation monitored by *operando* X-ray and infrared spectroscopies

Caroline Dessal, Thomas Len, Franck Morfin, Jean-Luc Rousset, Mimoun Aouine, Pavel Afanasiev, Laurent Piccolo*

Univ Lyon, Université Claude Bernard - Lyon 1, CNRS, IRCELYON - UMR 5256, 2 Avenue Albert Einstein, F-69626 VILLEURBANNE CEDEX, France.

ABSTRACT: Single-atom catalysts (SACs) are promising atom-efficient materials, with potentially superior performances with respect to their nanoparticulate counterparts. Owing to its practical importance and relative simplicity, CO oxidation on Pt/γ-Al_2O_3 is considered as an archetypal catalytic system. The efficiency of the corresponding SAC has recently been the subject of debate. In this work, in addition to systematic high-resolution scanning transmission electron microscopy, we have simultaneously monitored the Pt dispersion, oxidation state, and CO oxidation activity by *operando* fast X-ray absorption spectroscopy and diffuse reflectance infrared spectroscopy, both combined with mass spectrometry. It is shown that single Pt^{m+} atoms ($m \geq 2$), resulting from the standard impregnation-calcination procedure of SAC preparation, are poorly active. However, they gradually but irreversibly convert into highly active ~1-nm-sized $Pt^{\delta+}$ clusters ($\delta < 2$) throughout the heating/cooling reaction cycles, even under highly oxidizing conditions favorable to atomic dispersion. Increase in the Pt loading or the CO/O_2 concentration ratio accelerates the clustering-reduction phenomena. This work not only evidences a gradual aggregation/activation process for an important catalytic system, but also highlights the power of *operando* spectroscopies to address stability issues in single-atom catalysis.

Keywords

Single-atom catalysis; Pt/γ-Al2O3; operando spectroscopies; XAS; DRIFTS

INTRODUCTION

In the quest for minimal consumption of precious metals, single-atom heterogeneous catalysis has recently attracted much attention because single-atom catalysts (SACs) expose all the virtually active metal atoms to the reactants.[1–10] Moreover, with respect to supported nanoparticles, SACs can exhibit different performances in relation to their distinct electronic structure, onto which the support has a critical influence.[11] These materials have shown promising performances in a number of reactions related to energy, environment and chemicals production. However, owing to the inherent tendency of single atoms to aggregate into larger entities such as nanoparticles, SAC stability may be the main issue in future developments. For example, several works have shown the agglomeration tendency of Pt atoms on various supports under reducing atmospheres.[12–17] Nevertheless, whereas dynamical effects in catalysis have been investigated in detail for supported nanoparticles,[18,19] similar studies on SACs are still scarce. Noticeably, in many studies published so far, the metal dispersion (single atom or cluster/nanoparticle) during, or even after the reaction, is unknown, making the *in situ*/*operando* approaches[18,20–25] highly desirable. In this context, an atomic-scale understanding of SAC restructuring is expected to favor the design of stable SACs.[26]

A number of studies dedicated to Pt/Al_2O_3 SACs have been reported to date, with applications to CO oxidation, water-gas shift, and hydrocarbon processing.[27–32] CO oxidation on Pt/γ-Al_2O_3 can be considered as a reference model system due to its relative simplicity and practical relevance in e.g. air pollution control.[33] In a pioneer work on Pt_1/θ-Al_2O_3, Narula and coworkers concluded from infrared/X-ray absorption spectroscopies and scanning transmission electron microscopy (STEM) that Pt single atoms are intrinsically active toward CO oxidation.[30] A model based on density functional theory (DFT) suggested that Pt_1 prefers to bond to O_2 over CO, and that the reaction proceeds through a Pt carbonate. In contrast, Stair and coworkers concluded from infrared spectroscopy, temperature-programmed reaction and STEM that, unlike Pt nanoparticles, single Pt atoms supported on a variety of substrates including γ-Al_2O_3, are inactive for CO oxidation and water-gas shift reactions.[34] This was mostly ascribed to an excessively strong Pt_1-CO interaction.

In a recent work, we have shown from environmental STEM, X-ray absorption spectroscopy and DFT investigations that single Pt atoms on alumina are stabilized in oxygen atmosphere through the formation of Pt-O_{ads}-$Al_{support}$

bridges; in contrast, Pt atoms aggregate into mobile sub-nanometric clusters under hydrogen.[17] Here, we investigate the structural stability of Pt/γ-Al_2O_3 SACs throughout CO oxidation in correlation with their catalytic performances by using, in combination with STEM, state-of-the-art *operando* spectroscopies. We evidence that, even for relatively low Pt amounts and *a priori* favorable reaction conditions, single Pt atoms are prone to aggregate into clusters, which are much more active and then dominate the CO oxidation kinetics. This implies that, in metal/oxide SAC studies, even a low fraction of clusters or nanoparticles should not be neglected, as they may represent, depending on the considered reaction, the actual active species.

EXPERIMENTAL SECTION

Catalyst preparation

γ-Al_2O_3 powders (Sasol Puralox SCFa-140, >97.0 % Al_2O_3) were calcined in air at 600 °C for 3 h before use. For catalyst preparation by incipient wetness impregnation, 2.0 g of alumina was impregnated with 1.8 mL of an aqueous solution of $Pt(NH_3)_4(NO_3)_2$ (Alfa Aesar, >50 wt% Pt), dried in air at 60 °C for 5 h, and calcined in air (40 mL/min) at 300 °C for 2 h (2 °C/min ramp). The Pt loadings of the 0.3Pt and 1Pt samples were find equal to 0.31 wt% and 0.96 wt%, respectively, by inductively coupled plasma - optical emission spectroscopy (ICP-OES, Horiba Jobin Yvon).

Scanning transmission electron microscopy

The STEM-HAADF experiments were performed with a FEI Titan ETEM G2 electron microscope, equipped with a Cs image aberration corrector and operated at 300 keV. The extraction voltage, camera length, acceptance angles, STEM resolution and probe current were 4500 V, 245 mm, 29.2-146 °, 0.14 nm and <0.1 nA, respectively. For sample preparation, the powder was crushed and dispersed in ethanol through ultrasonication, dropped onto a holey carbon-coated 200 mesh Cu grid, and dried by a lamp. To avoid contamination during analysis and remove all residual carbon, the samples were Ar plasma-cleaned for 20 s (Plasma Prep 5, GaLa Instrumente). No filtering was applied on the STEM images.

Operando X-ray absorption spectroscopy

The local structure of Pt species was investigated by XAS in transmission mode on the ROCK beam line at the SOLEIL synchrotron. X-ray absorption spectra at the L3 edge of Pt were recorded. The powder samples were placed inside a pseudo plug-flow *operando* cell composed of a sample holder fitted into a heated block.[35] The cell was connected to a gas distribution system allowing for careful control of the gas flows at atmospheric pressure. *In situ* thermal treatments were applied from RT to 300 °C under air flow (10^5 Pa, 50 mL/min, 4 °C/min) or H_2 flow (10^5 Pa, 30 mL/min, 5 °C/min). Under the reaction mixture at atmospheric pressure (total flow rate 50 mL/min), the sample was heated at 2 °C/min from RT to 300 °C, and cooled down at the same rate. The gas mixture consisted of $CO:O_2$:He = 2:10:88% (COOX10 conditions) or $CO:O_2$:He = 2:2:96% (COOX2 conditions). The reactor was flushed for 10 minutes under He between the oxidative and the reductive treatments. Data merging and preliminary analysis were carried out using ATHENA software.[36] EXAFS fitting was performed using VIPER program.[37] The fit was performed alternatively in k and R spaces. When in the R space, it was done in the (Im + Module) mode, mathematically equivalent to the k-fit.

It should be noted that the error in Pt-Pt coordination number (CN) determination by EXAFS is high for these low-loaded and highly dispersed systems, because of the overlap between the Pt-Pt features and wiggles of the Pt-O FT signals. Thus, in the presence of several Pt-O bonds per Pt atom, determining the presence of less than one Pt neighbor is at the limit of the EXAFS technique. The second neighbor peak with a distance slightly above 3 Å is most probably due to the support Al atoms involved in the Pt-O-Al bonds. However, the high disorder of the Pt coordination environment makes it impossible to fit this contribution with an acceptable figure of merit.

Operando diffuse reflectance infrared Fourier transform spectroscopy

Operando infrared spectroscopy was performed using a Thermo Nicolet 6700 FTIR spectrophotometer equipped with a DRIFTS cell (Harrick HVC-DRP) and a high-sensitivity MCT detector. The cell, equipped with CaF_2 windows, was connected to a gas handling system allowing *in situ* treatments with several gases at temperatures up to 500 °C. About 30 mg of the powder sample was placed in the cell sample holder. The sample was submitted to the following treatments or reactions at atmospheric pressure with a total flow rate of 25 mL/min: (i) 20% O_2 in He, 2 °C/min, 350 °C, 2 h; (ii) 2% CO + 2 or 10% O_2 in He, 2 cycles; (iii) H_2, 2 °C/min, 350 °C, 2 h; (iv) identical to (ii); (v) identical to (i); (vi) identical to (ii). The spectra were recorded in the 1000–4000 cm^{-1} range at a resolution of 2 cm^{-1} by accumulating 64 scans. The Omnic software (Thermo) was used for initial data processing. Temperature cycles were composed of ramps (3 °C/min) and plateaus (20 min, for DRIFTS acquisition) every 50 °C. The reported temperature corresponds to that of the powder sample surface after calibration with a pyrometer. The gases exiting the DRIFTS cell were continuously monitored with a mass spectrometer (Aspec QMS from SRA Instruments). The experiments were also performed with bare γ-Al_2O_3 in order to subtract the signal of gaseous CO from the DRIFTS spectra.

Catalytic tests

The catalytic properties in CO oxidation were evaluated under atmospheric pressure in a continuous-flow fixed-bed reactor which consisted of a cylindrical glass tube (10 mm inner diameter) equipped with a sintered glass filter supporting the catalyst powder. The same quantity of Pt (0.5 mg) was used in all tests. The reactor was placed in a ceramic furnace heated or cooled at 1 °C/min between 50 °C and 280 °C. The catalyst temperature was recorded through a thermocouple immersed in the catalytic bed. By using mass-flow controllers, the gases were mixed ($CO:O_2$:He = 2:10:88% or 2:2:96%) and flowed through the reactor at a total rate of 50 Nml/min. The effluent gases

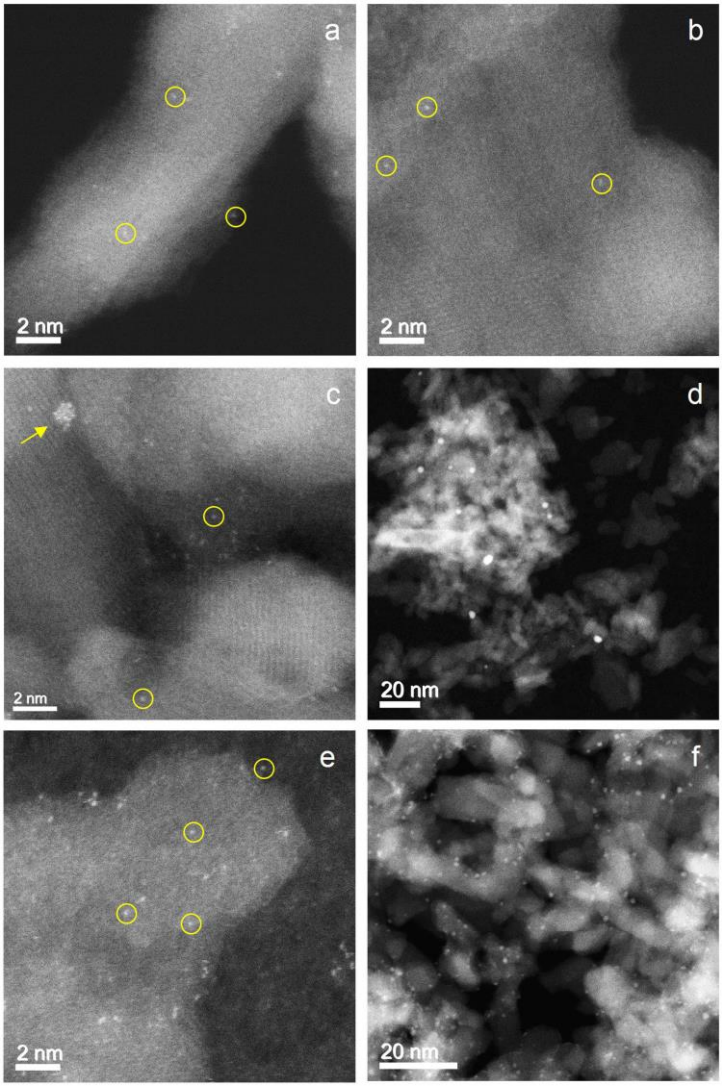

Figure 1. Representative STEM images of Pt/γ-Al_2O_3 samples throughout the catalysis experiments. (a-c) 0.3 wt% Pt/Al_2O_3 catalyst after calcination (a), subsequent CO oxidation cycle with CO:O_2 = 2:10% (b), and after full experiment (c). Average size of the clusters (such as that pointed by the arrow) in (c): 1.0 ± 0.3 nm. (d) 0.3 wt% Pt/Al_2O_3 catalyst after full experiment with CO:O_2 = 2:2%. Mostly Pt clusters are present (average size 1.9 ± 1.0 nm). (e-f) 1.0 wt% Pt/Al_2O_3 catalyst, as-prepared (e) and after full experiment with CO:O_2 = 2:10% (f). Mostly single Pt atoms are present in (e) and mostly Pt clusters (average size 1.0 ± 0.2 nm) are present in (f). Some of the single atoms are circled in yellow.

were analyzed online using a Micro GC equipped with a TCD detector.

RESULTS AND DISCUSSION

Two Pt/γ-Al_2O_3 catalysts were investigated, with a Pt loading of 0.3 wt% (0.3Pt sample) or 1.0 wt% (1Pt sample). Fig. 1 and Figs. S1-S3 show STEM images of the samples. For the as-prepared (i.e., calcined) samples, while 0.3Pt contains exclusively single Pt atoms (Fig. 1a), a mixture of single atoms and small clusters is present on 1Pt (Figs. 1e and S2a), consistently with previous reports.[17,27]

In order to compare the performances of these catalysts with those of pre-reduced ones, the samples were submitted to a series of successive reactive treatments under flow conditions at atmospheric pressure: (i) calcination in air, to accurately reset the initial (oxidized) conditions; (ii) CO oxidation reaction; (iii) reduction in hydrogen; (iv) CO oxidation (identical to ii). All four treatments were performed from RT up to 300 °C, followed by cooling back to RT. For the reaction stages, two sets of conditions were used, with CO:O_2 contents in helium of 2:10% (referred to as COOX10 conditions) or 2:2% (COOX2). Note that the COOX10 (more oxidizing) conditions were chosen to tentatively stabilize the SAC, given that it is stable under oxygen.[17] Similarly, pre-exposure to O_2 was shown to limit the H_2-induced sintering of Pt nanoparticles supported on alumina.[38] This protocol was similarly applied in a conventional flow-fixed-bed catalytic reactor, in *operando* DRIFTS-MS experiments, and in synchrotron-based *operando* XAS-MS experiments. In conventional testing (Fig.

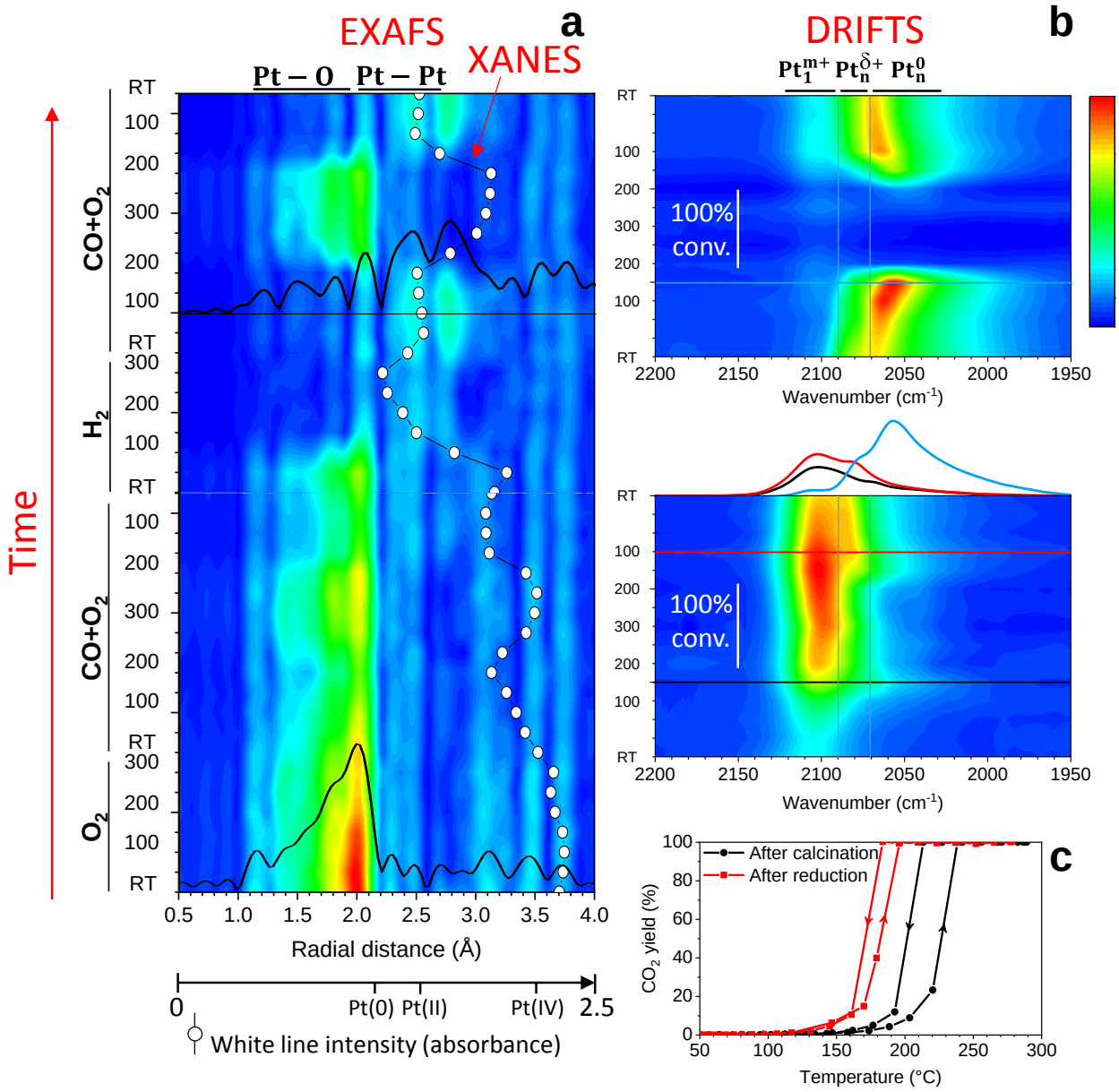

Figure 2. Monitoring of Pt species and their CO oxidation activity (0.3 wt% Pt/γ-Al_2O_3, CO:O_2 = 2:10%). (a) EXAFS color map showing the evolution with time (from bottom to top) of the FT throughout the calcination/reaction/reduction/reaction procedure. The full color scale corresponds to 0-2.13 $Å^{-4}$ in FT module. Two FT signals are shown in classical view. The radial distance is phase-corrected. The white disks represent the XANES white line intensity in the same experiment. The intensity values for Pt, $Pt(NH_3)_4(NO_3)_2$ and PtO_2 references (Fig. S11a) are reported on the bottom axis. (b) DRIFTS color map showing the evolution of the $\nu_{C\text{-}O}$ absorption band(s) in the Pt carbonyl wavenumber region during post-calcination (bottom panel) and post-reduction (top panel) reaction steps. The full color scales correspond to 0-0.10 (bottom) and 0-0.18 (top) in absorbance. Three spectra corresponding to the horizontal lines (at 150 °C during heating and 100 °C during cooling) on the DRIFTS maps are plotted in classical view. The 100% CO conversion region, as derived from mass spectrometry, is indicated. In (a) and (b), the Y-axes show temperatures in °C. (c) CO oxidation light off curves obtained in a conventional flow-fixed-bed reactor following a similar protocol as in *operando* experiments.

S4) and DRIFTS (Figs. S5-S7), two heating-cooling CO oxidation cycles (instead of one for XAS) were performed at each reaction stage in order to assess the catalyst stability.

Figure 2 displays the results of such an investigation for the 0.3Pt sample under oxygen-rich COOX10 reaction conditions. In addition to Fig. 2b, a conventional view of the Pt-carbonyl region of DRIFTS spectra is shown in Fig. S8 (left panels). The corresponding data for 1Pt COOX10 (Fig. S9) and 0.3Pt COOX2 (Fig. S10) are reported in Supporting Information, together with XANES and EXAFS references (Fig. S11), and additional XAS raw data and analyses (Figs. S12-S15, Tables S1-S3).

Pre-oxidized single Pt atoms

In the as-prepared (air-calcined) SAC, the EXAFS Fourier transform only shows a Pt-O contribution ($r \approx 2.0$ Å, Fig. 2a) without any Pt-Pt one, confirming the absence of metallic Pt clusters, in accordance with previous works.[17,30] Comparison of the XANES of the SAC with those of bulk Pt, bulk PtO_2, and pure $Pt(NH_3)_4(NO_3)_2$ precursor references (Fig. S11a) suggests an oxidation degree of the single Pt atoms comprised between II (Pt precursor) and IV (PtO_2).

During the first CO oxidation cycle (bottom of Fig. 2a), the main EXAFS contribution remains the Pt-O one. At first sight, the first CO oxidation run (heating) is performed on single Pt atoms, which show a moderate activity with a half-conversion temperature $T_{1/2} \approx 230$ °C in a conventional flow-fixed-bed reactor (Figs. 2c and S4a). Upon cooling, $T_{1/2}$ decreases to *ca*. 200 °C. The resulting hysteresis is mainly explained in the literature by mass or heat diffusion effects, low-temperature poisoning of Pt by CO, and different oxidation states of Pt in light-off and extinction stages, which can be coupled to each other.[33,39,40] Looking closely at the EXAFS evolution, small Pt-Pt features are visible at 150-200 °C during heating. Then, the Pt-Pt feature becomes more clearly visible during cooling, in the 150 °C-RT temperature region. The presence of Pt-Pt features is correlated to minima in the XANES white line intensity (WLI), represented horizontally in Fig. 2a. The Pt-Pt feature appearance in EXAFS and WLI decrease in XANES indicate Pt clustering and reduction.

Another indication of Pt clustering comes from DRIFTS monitoring (Figs. 2b and S8). While the main peak at 2106-2100 cm^{-1} is ascribed to CO linearly adsorbed on single Pt^{m+} cations ($m \geq 2$), the shoulder at 2090-2070 cm^{-1}, present at ca. 150 °C on heating and at 150-50 °C on cooling, can be ascribed to partially oxidized Pt clusters ($Pt^{\delta+}$, $\delta < 2$).[34,39] Unlike the main band, this shoulder shifts towards higher wavenumbers as temperature decreases, due to the increased dipole-dipole coupling between CO adsorbates.[41] Furthermore, the disappearance of this contribution -and this contribution only- throughout the full CO conversion period suggests that the precursor of the active species is $Pt^{\delta+}$. This small fraction of Pt clusters would coexist with poorly active single Pt cations, the DRIFTS signature of which appears indeed essentially unaffected by the reaction. Indeed, no decrease of the Pt^{m+}-CO band intensity was observed at high CO conversion (Fig. 2b). However, a slight decrease in this single-atom contribution was observed at high CO conversion in the second CO oxidation cycle (Fig. S5), and more markedly under oxygen-poor COOX2 conditions (Fig. S7). In these cases the Pt clusters are majority species, and the decreasing amounts of SAs could be expected. Nevertheless, unlike the $Pt^{\delta+}$-CO (clusters), the Pt^{m+}-CO species (SAs) never disappear completely, thus the depletions can be ascribed to desorption and not necessarily to reaction. Further, the ~2100 cm^{-1} band (SAs) actually increases on heating, and decreases back at the end of the cycle (Fig. 2b). Such an evolution indicates that single Pt atoms can hardly accommodate both CO and oxygen and that the adsorption competition is favorable to oxygen at low temperature and to CO at higher temperatures, at which the reaction proceeds on the clusters. This partly reconciles the results of Moses DeBusk *et al.* and Ding *et al.*, who found that single Pt atoms prefer to accommodate oxygen or CO, respectively.[30,34] Pt clustering appears even more marked during the second DRIFTS cycle (Fig. S5), and it correlates with a higher activity (lower $T_{1/2}$, Fig. S4a). However, at the end of the CO oxidation cycles, a large proportion of single Pt atoms remains, consistently with STEM analyses (Fig. 1b).

Remarkably, some authors have proposed, using DFT calculations, CO oxidation mechanisms on $Pt/Al_2O_3(010)$ SACs, which involve either $Pt(CO_3)$ [30] or Pt (O-O-C=O) [42] species. The former has also been considered by Newton *et al*. to interpret their transient experiments on commercial Pt/Al_2O_3 catalysts.[43,44] Our simultaneous monitoring of the catalyst state and light-off activity, based for the first time on *operando* experiments, shows that the involvement of Pt carbonates is not required (though not ruled out) to explain our data. In our conditions, the oxidation of CO to CO_2 can proceed through the conventional Langmuir-Hinshelwood mechanism over the fraction of Pt clusters formed *in situ* within the initial SAC. The increase of this cluster fraction throughout CO oxidation cycles leads to an increase in the CO oxidation activity. Our results are consistent with those of Ding *et al*.[34] and of Lou and Liu,[45] who concluded on the inactivity or poor activity, respectively, of Pt single atoms supported on γ-Al_2O_3,. In connection to these findings, the superiority of subnanometric clusters overs single atoms was previously reported for CO oxidation over Ir/FeO_x.[46]

Pre-reduced Pt clusters

The second part of the experiments consisted in a reducing treatment in hydrogen in order to obtain a majority of Pt clusters,[17] followed by an additional CO oxidation cycle (or two in the cases of DRIFTS and conventional tests). Fig.2a shows the gradual disappearance of the Pt-O EXAFS feature during the hydrogen treatment, together with the decrease in the XANES WLI and the appearance of a small Pt-Pt contribution ($r \approx 2.6$ Å). As previously reported, such a treatment of a Pt/γ-Al_2O_3 SAC leads to a dominant fraction of 0.9 nm-sized Pt clusters[13,17] (see also Fig. S2c,d for 1Pt sample). The Pt-Pt CN was close to 6 (Table S1), in agreement with the calculations of Jentys for 13-atom spherical clusters.[47] The Pt-Pt CN remains roughly constant under CO/O_2 at low temperature, up to 150 °C, i.e. before the light-off. DRIFTS supports the quasi exclusive presence of reduced Pt clusters in these conditions, as attested by the 2070-2050 cm^{-1} feature corresponding to linear Pt^0-CO adsorption, with clear coverage-dependent band shift.[48] A fraction of partially oxidized Pt also exists (shoulder at ca. 2080 cm^{-1}, better seen in Fig. S8), which is assigned to $Pt^{\delta+}$ multimers and/or cluster periphery sites. The sudden disappearance of the 2070-2050 cm^{-1} DRIFTS feature upon light-off (Fig. 2b and S8) shows again that the Pt clusters –now majority– are the catalytically active species. This pre-reduced catalyst is much more active than the pre-calcined one, with a decrease of $T_{1/2}$ by 52 °C (Figs.

2c and S4). The amplification of activity is ascribed to the increased fraction of Pt clusters. The level of the XANES WLI under reaction conditions (Fig. 2a) suggests that these active Pt clusters are oxidized.

However, no Pt-Pt contribution is present in the EXAFS signal during the 100% CO conversion period, while the Pt-O component ($r \approx 2.0$ Å) and the WLI are reinforced (Fig. 2a). This is ascribed to the oxidation of the Pt clusters into amorphous PtO_x. Indeed, when 100% CO conversion is achieved, in the major part of the catalyst bed, the gaseous atmosphere contains only inert gas and O_2, thus being highly oxidative. In order to confirm this hypothesis, as opposed to an oxidative redispersion of the Pt clusters into single Pt cations, a quenching experiment was carried out during conventional catalytic tests (on the 1Pt sample, which shows a similar behavior as 0.3Pt, see Fig. S9). At the end of the COOX10 heating ramp, after a plateau of 25 min at 280 °C, the reactor was quickly water-cooled to RT under air and the sample was analyzed by STEM. Fig. S2e,f clearly shows Pt clusters with an average size of 1.1 ± 0.3 nm, which supports the hypothesis that the Pt clusters are not redispersed but oxidized during the reaction at high temperature, i.e. at 100% CO conversion.

Upon return to low temperature under CO oxidation conditions, the reinforcement of the DRIFTS feature at ca. 2100 cm^{-1} (Figs. 2b and S8, top panels), which had appeared at 150 °C upon heating, is most likely due to CO adsorption on remaining single Pt^{m+} cations. Although present in much smaller fraction after reduction, these species behave similarly as before reduction towards CO adsorption. Indeed, as previously mentioned, an increase of the 2100-2110 cm^{-1} feature (single Pt cations after calcination) upon heating up to 300 °C and subsequent cooling down to 150 °C was observed (Figs. 2b and S8, bottom panels).

However, most of the signal (2080-2050 cm^{-1}) is ascribable to Pt clusters. Unlike before the reduction treatment (cycles 1 and 2), after reduction two successive CO oxidation cycles produce similar DRIFTS signals (Fig. S5, cycles 3 and 4), consistently with the catalytic tests (Fig. S4). This indicates that the clustering process is complete. At the end of the whole process, Pt is thus mostly returned into the form of Pt^0 and, to lower extent, $Pt^{\delta+}$ clusters (low XANES intensity and CN = 6, see Table S1). However, a significant proportion of single Pt atoms (Pt^{m+}) remains, as seen from EXAFS and DRIFTS (Fig. 2a) and post-reaction STEM (Figs. 1c and S1d-f). In DRIFTS experiments, after the first two stages (post-calcination and post-reduction), the catalyst was further calcined *in situ* under air flow and two additional CO oxidation cycles (5 and 6, Fig. S5) were performed. The DRIFTS data overall appear very similar to those of the post-reduction stage. This implies that the clustering process, which begins after the initial calcination, and completes after reduction, is irreversible.

Effect of Pt loading and reaction conditions

When comparing the results for 0.3Pt COOX10 (Fig. 2) with those for 1Pt COOX10 (Fig. S9) and 0.3Pt COOX2 (Fig. S10), all three processes look qualitatively similar. However, DRIFTS evidences that the fraction of metallic Pt clusters in the first reaction stage is more important at higher Pt loading (1Pt COOX10), and even more under less oxidizing conditions (0.3Pt COOX2). Consistently with the above conclusion that Pt clusters are more active than single atoms, $T_{1/2}$ is decreased by 24 °C at higher Pt loading under COOX10 conditions (Fig. S4). In contrast, after the reduction treatment leading to a majority of Pt clusters in all cases, the DRIFTS data are almost identical for 0.3Pt and 1Pt, and accordingly the COOX10 activities are now similar. The activity of 0.3Pt is lower under COOX2 conditions ($T_{1/2}$ = 239 °C, vs. 226 °C for COOX10) because of the limited supply in O_2 induced by strong CO adsorption at low temperature, i.e. negative reaction order in CO, similarly to what is known for larger Pt particles within the Langmuir-Hinshelwood mechanism.[49] In all the cases, as shown by Figs. S5-S7 (cycles 3-6 vs cycles 1-2), the adsorption of CO as measured by DRIFTS is much more prominent on pre-reduced catalysts (Pt clusters) than on pre-oxidized ones (single Pt atoms).

Fig. 3 summarizes the results and allows a quantitative comparison of the evolutions of the white line intensities (a) and Pt-Pt coordination numbers (b) between the three cases. Both show large variations throughout the experiment. The WLI is maximum under highly oxidizing conditions, i.e. calcination treatment and high reaction temperature (high CO conversion). It decreases under less oxidizing conditions, i.e. reduction treatment and low reaction temperature. The WLI decrease corresponds to concomitant decrease of Pt-O CNs in EXAFS, from more than 5 to less than 1 (Fig. S12 and Tables S1-S3). As expected, the WLI and the Pt-O CN show very similar trends (Fig. S12). Overall, Fig. 3 evidences clear Pt reduction (a) and Pt clustering (b) tendencies. Switching from 0.3Pt-COOX10 conditions to 1Pt-COOX10 or 0.3Pt-COOX2 leads to a decrease in the WLI, i.e. both the increase in Pt loading and the decrease in oxygen concentration have Pt reduction effects. The Pt-Pt bonds corresponding to few-atom clusters are already detected in EXAFS from ~100 °C upon heating in 1Pt-COOX10 and 0.3Pt-COOX2 experiments, whereas for 0.3Pt-COOX10 the Pt clusters appear only below 200 °C on cooling. However, the COOX2 conditions induce a larger increase in CN in the first reaction cooling stage, with a maximum CN of 5 vs. 3-4 for the COOX10 conditions. Therefore, more reducing (COOX2) conditions lead to a larger number of Pt atoms in the clusters.

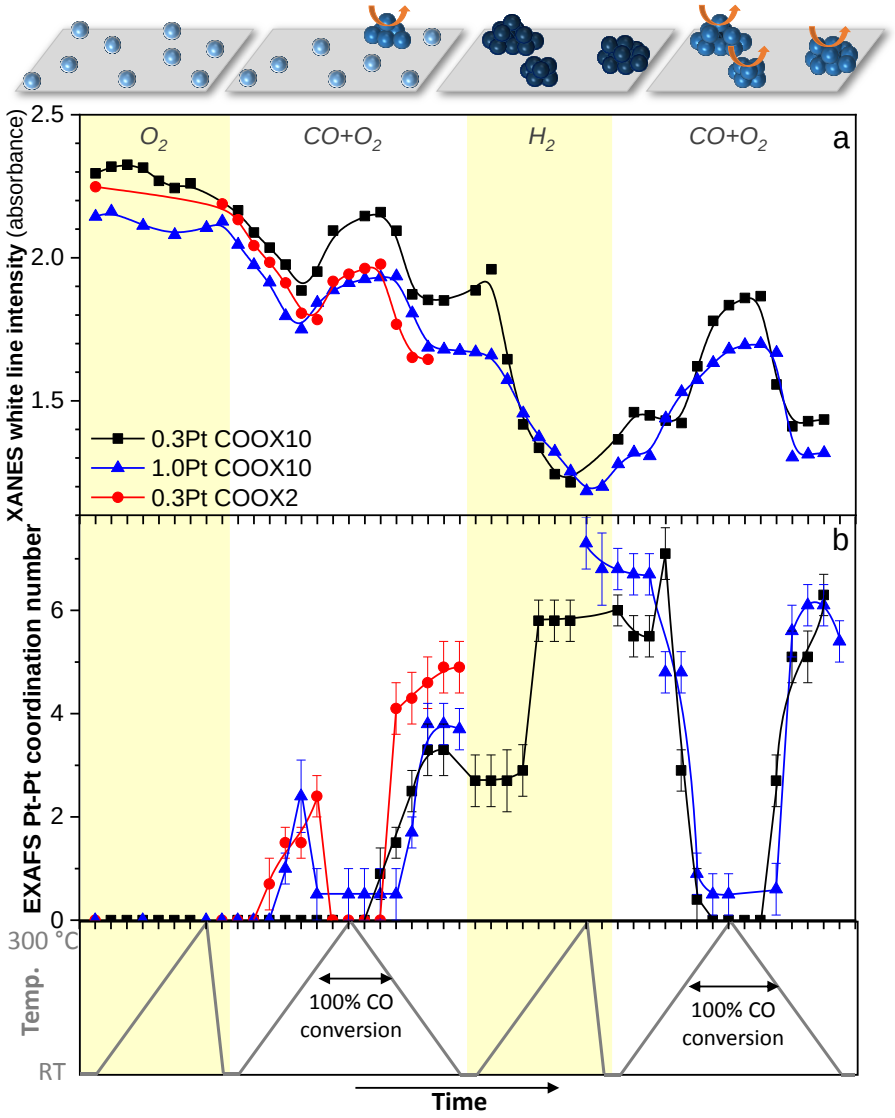

Figure 3. Evolution of XANES white line intensities (a) and Pt-Pt coordination numbers derived from EXAFS analysis (b) during the calcination/reaction/reduction/reaction sequence on 0.3 wt% Pt/γ-Al_2O_3 (COOX10 and COOX2 conditions) and 1.0 wt% Pt/γ-Al_2O_3 (COOX10). The total duration of each experiment was ~20 h, except in COOX2 for which only the first half was carried out. The drawings represent the catalyst state. The ball color represents the oxidation state of Pt, going from highly cationic (light blue) to slightly cationic (medium blue) and reduced (dark blue). Orange arrows represent CO oxidation. The double black arrows at the bottom of the figure indicate the approximate full-CO-conversion temperature regions.

CONCLUSIONS

In this work, in addition to conventional catalytic testing and STEM, we have used *operando* XAS and DRIFTS spectroscopies to investigate the oxidation of CO over a 0.3 wt% Pt/γ-Al_2O_3 SAC prepared by incipient wetness impregnation-calcination. The SAC behavior has been compare d to its pre-reduced and 1 w t% counter parts under both standard ($CO:O_2$ = 2:2 wt%) and highly oxidizing ($CO:O_2$ = 2:10 wt%) conditions.

It is shown that the initially single Pt cations gradually aggregate into partially oxidized Pt clusters in the course of the reaction light-off/light-out cycles. The single atoms are strongly coordinated to oxygen at room temperature, and to CO at higher temperature. Such a strong adsorption prevents the SAs from catalyzing the reaction. As the clusters are more active than the single atoms, their formation during the reaction, and upon hydrogen treatment, leads to increases in the CO oxidation activity. As compared to the low-loaded SAC, the 1 wt% Pt catalyst shows a larger proportion of clusters, a lower average oxidation state, and a higher Pt-specific activity. Similarly, exposing the SAC to less oxidizing conditions deeply increases the cluster fraction and decreases the oxidation state.

While demonstrating the clustering dynamics of Pt atoms from a systematic multi-technique investigation, this work enriches the debate on the CO oxidation activity of

$Pt_1/\gamma\text{-}Al_2O_3$ SACs. These results are likely to be qualitatively applicable to other catalytic systems and demonstrate the value of *operando* investigations to assess the intrinsic activity-stability of SACs.

ASSOCIATED CONTENT

Supporting Information. Additional STEM, DRIFTS, XAS, and CO oxidation data.
This material is available free of charge via the Internet at http://pubs.acs.org.

AUTHOR INFORMATION

Corresponding Author

* E-mail: Laurent.Piccolo@ircelyon.univ-lyon1.fr

Notes

The authors declare no competing financial interests.

ACKNOWLEDGMENT

S. Belin (SOLEIL), C. Zlotea and A. Malouche (ICMPE) are acknowledged for support with XAS experiments at the ROCK beamline of SOLEIL synchrotron (proposal 20170160). L. Roiban (MATEIS) is acknowledged for help in TEM experiments. N. Cristin and P. Mascunan (IRCELYON) are acknowledged for ICP analyses. Agence Nationale de la Recherche (UltraCat project, ANR-17-CE06-0008), Région Auvergne-Rhône Alpes (CMIRA 2016 project) and LABEX iMUST ANR-10-LABX-0064/ ANR-11-IDEX-0007 are acknowledged for financial support. The XAS work was supported by a public grant overseen by the French National Research Agency (ANR) as part of the "Investissements d'Avenir" program (ANR-10-EQPX45). CLYM is acknowledged for access to the FEI Titan microscope.

REFERENCES AND NOTES

(1) Qiao, B.; Wang, A.; Yang, X.; Allard, L. F.; Jiang, Z.; Cui, Y.; Liu, J.; Li, J.; Zhang, T. Single-Atom Catalysis of CO Oxidation Using Pt_1/FeO_x. *Nat. Chem.* **2011**, *3* (8), 634–641. https://doi.org/10.1038/nchem.1095.

(2) Li, Z.-Y.; Yuan, Z.; Li, X.-N.; Zhao, Y.-X.; He, S.-G. CO Oxidation Catalyzed by Single Gold Atoms Supported on Aluminum Oxide Clusters. *J. Am. Chem. Soc.* **2014**, *136* (40), 14307–14313. https://doi.org/10.1021/ja508547z.

(3) Wei, H.; Liu, X.; Wang, A.; Zhang, L.; Qiao, B.; Yang, X.; Huang, Y.; Miao, S.; Liu, J.; Zhang, T. FeO_x-Supported Platinum Single-Atom and Pseudo-Single-Atom Catalysts for Chemoselective Hydrogenation of Functionalized Nitroarenes. *Nat. Commun.* **2014**, *5*, 5634. https://doi.org/10.1038/ncomms6634.

(4) Yan, H.; Cheng, H.; Yi, H.; Lin, Y.; Yao, T.; Wang, C.; Li, J.; Wei, S.; Lu, J. Single-Atom Pd_1/Graphene Catalyst Achieved by Atomic Layer Deposition: Remarkable Performance in Selective Hydrogenation of 1,3-Butadiene. *J. Am. Chem. Soc.* **2015**, *137* (33), 10484–10487. https://doi.org/10.1021/jacs.5b06485.

(5) Jones, J.; Xiong, H.; DeLaRiva, A. T.; Peterson, E. J.; Pham, H.; Challa, S. R.; Qi, G.; Oh, S.; Wiebenga, M. H.; Pereira Hernandez, X. I.; et al. Thermally Stable Single-Atom Platinum-on-Ceria Catalysts via Atom Trapping. *Science* **2016**, *353* (6295), 150–154. https://doi.org/10.1126/science.aaf8800.

(6) Caparrós, F. J.; Soler, L.; Rossell, M. D.; Angurell, I.; Piccolo, L.; Rossell, O.; Llorca, J. Remarkable Carbon Dioxide Hydrogenation to Ethanol on a Palladium/Iron Oxide Single-Atom Catalyst. *ChemCatChem* **2018**, *10* (11), 2365–2369. https://doi.org/10.1002/cctc.201800362.

(7) Liu, J. Catalysis by Supported Single Metal Atoms. *ACS Catal.* **2017**, *7*, 34–59. https://doi.org/10.1021/acscatal.6b01534.

(8) Wang, A.; Li, J.; Zhang, T. Heterogeneous Single-Atom Catalysis. *Nat. Rev. Chem.* **2018**, *2* (6), 65–81. https://doi.org/10.1038/s41570-018-0010-1.

(9) Cui, X.; Li, W.; Ryabchuk, P.; Junge, K.; Beller, M. Bridging Homogeneous and Heterogeneous Catalysis by Heterogeneous Single-Metal-Site Catalysts. *Nat. Catal.* **2018**, *1* (6), 385–397. https://doi.org/10.1038/s41929-018-0090-9.

(10) Lang, R.; Xi, W.; Liu, J.-C.; Cui, Y.-T.; Li, T.; Lee, A. F.; Chen, F.; Chen, Y.; Li, L.; Li, L.; et al. Non Defect-Stabilized Thermally Stable Single-Atom Catalyst. *Nat. Commun.* **2019**, *10* (1), 234. https://doi.org/10.1038/s41467-018-08136-3.

(11) Chen, Y.; Huang, Z.; Ma, Z.; Chen, J.; Tang, X. Fabrication, Characterization, and Stability of Supported Single-Atom Catalysts. *Catal. Sci. Technol.* **2017**, *7* (19), 4250–4258. https://doi.org/10.1039/C7CY00723J.

(12) Bradley, S. A.; Sinkler, W.; Blom, D. A.; Bigelow, W.; Voyles, P. M.; Allard, L. F. Behavior of Pt Atoms on Oxide Supports During Reduction Treatments at Elevated Temperatures, Characterized by Aberration Corrected Stem Imaging. *Catal. Lett.* **2012**, *142* (2), 176–182. https://doi.org/10.1007/s10562-011-0756-2.

(13) Sinkler, W.; Sanchez, S. I.; Bradley, S. A.; Wen, J.; Mishra, B.; Kelly, S. D.; Bare, S. R. Aberration-Corrected Transmission Electron Microscopy and in Situ XAFS Structural Characterization of $Pt/\gamma\text{-}Al_2O_3$ Nanoparticles. *ChemCatChem* **2015**, *7* (22), 3779–3787. https://doi.org/10.1002/cctc.201500784.

(14) Nagai, Y.; Dohmae, K.; Ikeda, Y.; Takagi, N.; Tanabe, T.; Hara, N.; Guilera, G.; Pascarelli, S.; Newton, M. A.; Kuno, O.; et al. In Situ Redispersion of Platinum Autoexhaust Catalysts: An On-Line Approach to Increasing Catalyst Lifetimes? *Angew. Chem. Int. Ed.* **2008**, *47* (48), 9303–9306. https://doi.org/10.1002/anie.200803126.

(15) Gänzler, A. M.; Casapu, M.; Vernoux, P.; Loridant, S.; Cadete Santos Aires, F. J.; Epicier, T.; Betz, B.; Hoyer, R.; Grunwaldt, J.-D. Tuning the Structure of Platinum Particles on Ceria In Situ for Enhancing the Catalytic Performance of Exhaust Gas Catalysts. *Angew. Chem. Int. Ed.* **2017**, *56* (42), 13078–13082. https://doi.org/10.1002/anie.201707842.

(16) Duan, S.; Wang, R.; Liu, J. Stability Investigation of a High Number Density Pt_1/Fe_2O_3 Single-Atom Catalyst under Different Gas Environments by HAADF-STEM. *Nanotechnol.* **2018**, *29* (20), 204002. https://doi.org/10.1088/1361-6528/aab1d2.

(17) Dessal, C.; Sangnier, A.; Chizallet, C.; Dujardin, C.; Morfin, F.; Rousset, J.-L.; Aouine, M.; Bugnet, M.; Afanasiev, P.; Piccolo, L. Atmosphere-Dependent Stability and Mobility of Catalytic Pt Single Atoms and Clusters on $\gamma\text{-}Al_2O_3$. *Nanoscale* **2019**, *11* (14), 6897–6904. https://doi.org/10.1039/C9NR01641D.

(18) Lira, E.; Merte, L. R.; Behafarid, F.; Ono, L. K.; Zhang, L.; Roldan Cuenya, B. Role and Evolution of Nanoparticle Structure and Chemical State during the Oxidation of NO over Size- and Shape-Controlled $Pt/\gamma\text{-}Al_2O_3$ Catalysts under Operando Conditions. *ACS Catal.* **2014**, *4* (6), 1875–1884. https://doi.org/10.1021/cs500137r.

(19) Zhai, H.; Alexandrova, A. N. Fluxionality of Catalytic Clusters: When It Matters and How to Address It. *ACS Catal.* **2017**, *7* (3), 1905–1911. https://doi.org/10.1021/acscatal.6b03243.

(20) Frenken, J.; Groot, I. *Operando Research in Heterogeneous Catalysis*, 1st ed. 2017.; Springer International Publishing AG: New York, NY, 2017.

(21) Kaftan, A.; Kollhoff, F.; Nguyen, T.-S.; Piccolo, L.; Laurin, M.; Libuda, J. Sensitivity of CO Oxidation toward Metal

Oxidation State in Ceria-Supported Catalysts: An Operando DRIFTS-MS Study. *Catal. Sci. Technol.* **2016**, *6* (3), 818–828. https://doi.org/10.1039/C5CY00827A.

(22) Zlotea, C.; Oumellal, Y.; Provost, K.; Morfin, F.; Piccolo, L. Role of Hydrogen Absorption in Supported Pd Nanocatalysts during CO-PROX: Insights from Operando X-Ray Absorption Spectroscopy. *Appl. Catal. B* **2018**, *237*, 1059–1065. https://doi.org/10.1016/j.apcatb.2018.06.059.

(23) Asakura, H.; Hosokawa, S.; Ina, T.; Kato, K.; Nitta, K.; Uera, K.; Uruga, T.; Miura, H.; Shishido, T.; Ohyama, J.; et al. Dynamic Behavior of Rh Species in Rh/Al2O3 Model Catalyst during Three-Way Catalytic Reaction: An Operando X-Ray Absorption Spectroscopy Study. *J. Am. Chem. Soc.* **2018**, *140* (1), 176–184. https://doi.org/10.1021/jacs.7b07114.

(24) Zhang, S.; Tang, Y.; Nguyen, L.; Zhao, Y.-F.; Wu, Z.; Goh, T.-W.; Liu, J. J.; Li, Y.; Zhu, T.; Huang, W.; et al. Catalysis on Singly Dispersed Rh Atoms Anchored on an Inert Support. *ACS Catal.* **2018**, *8* (1), 110–121. https://doi.org/10.1021/acscatal.7b01788.

(25) Liu, L.; Zakharov, D. N.; Arenal, R.; Concepcion, P.; Stach, E. A.; Corma, A. Evolution and Stabilization of Subnanometric Metal Species in Confined Space by in Situ TEM. *Nat. Commun.* **2018**, *9* (1), 574. https://doi.org/10.1038/s41467-018-03012-6.

(26) Qin, R.; Liu, P.; Fu, G.; Zheng, N. Strategies for Stabilizing Atomically Dispersed Metal Catalysts. *Small Methods* **2018**, *2* (1), 1700286. https://doi.org/10.1002/smtd.201700286.

(27) Kwak, J. H.; Hu, J.; Mei, D.; Yi, C.-W.; Kim, D. H.; Peden, C. H. F.; Allard, L. F.; Szanyi, J. Coordinatively Unsaturated Al^{3+} Centers as Binding Sites for Active Catalyst Phases of Platinum on γ-Al_2O_3. *Science* **2009**, *325* (5948), 1670–1673. https://doi.org/10.1126/science.1176745.

(28) Mei, D.; Kwak, J. H.; Hu, J.; Cho, S. J.; Szanyi, J.; Allard, L. F.; Peden, C. H. F. Unique Role of Anchoring Penta-Coordinated Al^{3+} Sites in the Sintering of γ-Al_2O_3-Supported Pt Catalysts. *J. Phys. Chem. Lett.* **2010**, *1* (18), 2688–2691. https://doi.org/10.1021/jz101073p.

(29) Zhai, Y.; Pierre, D.; Si, R.; Deng, W.; Ferrin, P.; Nilekar, A. U.; Peng, G.; Herron, J. A.; Bell, D. C.; Saltsburg, H.; et al. Alkali-Stabilized Pt-OHx Species Catalyze Low-Temperature Water-Gas Shift Reactions. *Science* **2010**, *329* (5999), 1633–1636. https://doi.org/10.1126/science.1192449.

(30) Moses-DeBusk, M.; Yoon, M.; Allard, L. F.; Mullins, D. R.; Wu, Z.; Yang, X.; Veith, G.; Stocks, G. M.; Narula, C. K. CO Oxidation on Supported Single Pt Atoms: Experimental and Ab Initio Density Functional Studies of CO Interaction with Pt Atom on θ-Al_2O_3(010) Surface. *J. Am. Chem. Soc.* **2013**, *135* (34), 12634–12645. https://doi.org/10.1021/ja401847c.

(31) Zhang, Z.; Zhu, Y.; Asakura, H.; Zhang, B.; Zhang, J.; Zhou, M.; Han, Y.; Tanaka, T.; Wang, A.; Zhang, T.; et al. Thermally Stable Single Atom Pt/m-Al_2O_3 for Selective Hydrogenation and CO Oxidation. *Nat. Commun.* **2017**, *8*, 16100. https://doi.org/10.1038/ncomms16100.

(32) Cui, X.; Junge, K.; Dai, X.; Kreyenschulte, C.; Pohl, M.-M.; Wohlrab, S.; Shi, F.; Brückner, A.; Beller, M. Synthesis of Single Atom Based Heterogeneous Platinum Catalysts: High Selectivity and Activity for Hydrosilylation Reactions. *ACS Cent. Sci.* **2017**, *3* (6), 580–585. https://doi.org/10.1021/acscentsci.7b00105.

(33) Morfin, F.; Nguyen, T.-S.; Rousset, J.-L.; Piccolo, L. Synergy between Hydrogen and Ceria in Pt-Catalyzed CO Oxidation: An Investigation on Pt–CeO2 Catalysts Synthesized by Solution Combustion. *Appl. Catal. B* **2016**, *197*, 2–13. https://doi.org/10.1016/j.apcatb.2016.01.056.

(34) Ding, K.; Gulec, A.; Johnson, A. M.; Schweitzer, N. M.; Stucky, G. D.; Marks, L. D.; Stair, P. C. Identification of Active Sites in CO Oxidation and Water-Gas Shift over Supported Pt Catalysts. *Science* **2015**, *350* (6257), 189–192. https://doi.org/10.1126/science.aac6368.

(35) La Fontaine, C.; Barthe, L.; Rochet, A.; Briois, V. X-Ray Absorption Spectroscopy and Heterogeneous Catalysis: Performances at the SOLEIL's SAMBA Beamline. *Catal. Today* **2013**, *205*, 148–158. https://doi.org/10.1016/j.cattod.2012.09.032.

(36) Ankudinov, A. L.; Ravel, B.; Rehr, J. J.; Conradson, S. D. Real-Space Multiple-Scattering Calculation and Interpretation of x-Ray-Absorption near-Edge Structure. *Phys. Rev. B* **1998**, *58* (12), 7565–7576. https://doi.org/10.1103/PhysRevB.58.7565.

(37) Klementev, K. V. Extraction of the Fine Structure from X-Ray Absorption Spectra. *J. Phys. D: Appl. Phys.* **2001**, *34* (2), 209. https://doi.org/10.1088/0022-3727/34/2/309.

(38) Matos, J.; Ono, L. K.; Behafarid, F.; Croy, J. R.; Mostafa, S.; DeLaRiva, A. T.; Datye, A. K.; Frenkel, A. I.; Roldan Cuenya, B. In Situ Coarsening Study of Inverse Micelle-Prepared Pt Nanoparticles Supported on γ-Al_2O_3: Pretreatment and Environmental Effects. *Phys. Chem. Chem. Phys.* **2012**, *14* (32), 11457–11467. https://doi.org/10.1039/C2CP41339F.

(39) Carlsson, P.-A.; Österlund, L.; Thormählen, P.; Palmqvist, A.; Fridell, E.; Jansson, J.; Skoglundh, M. A Transient in Situ FTIR and XANES Study of CO Oxidation over Pt/Al_2O_3 Catalysts. *J. Catal.* **2004**, *226* (2), 422–434. https://doi.org/10.1016/j.jcat.2004.06.009.

(40) Casapu, M.; Fischer, A.; Gänzler, A. M.; Popescu, R.; Crone, M.; Gerthsen, D.; Türk, M.; Grunwaldt, J.-D. Origin of the Normal and Inverse Hysteresis Behavior during CO Oxidation over Pt/Al_2O_3. *ACS Catal.* **2017**, *7* (1), 343–355. https://doi.org/10.1021/acscatal.6b02709.

(41) Primet, M. Electronic Transfer and Ligand Effects in the Infrared Spectra of Adsorbed Carbon Monoxide. *J. Catal.* **1984**, *88* (2), 273–282. https://doi.org/10.1016/0021-9517(84)90003-4.

(42) Gao, H. CO Oxidation Mechanism on the γ-Al2O3 Supported Single Pt Atom: First Principle Study. *Appl. Surf. Sci.* **2016**, *379*, 347–357. https://doi.org/10.1016/j.apsusc.2016.04.009.

(43) Newton, M. A.; Ferri, D.; Smolentsev, G.; Marchionni, V.; Nachtegaal, M. Room-Temperature Carbon Monoxide Oxidation by Oxygen over Pt/Al_2O_3 Mediated by Reactive Platinum Carbonates. *Nat. Commun.* **2015**, *6*, 8675. https://doi.org/10.1038/ncomms9675.

(44) Newton, M. A.; Ferri, D.; Smolentsev, G.; Marchionni, V.; Nachtegaal, M. Kinetic Studies of the Pt Carbonate-Mediated, Room-Temperature Oxidation of Carbon Monoxide by Oxygen over Pt/Al_2O_3 Using Combined, Time-Resolved XAFS, DRIFTS, and Mass Spectrometry. *J. Am. Chem. Soc.* **2016**, *138* (42), 13930–13940. https://doi.org/10.1021/jacs.6b06819.

(45) Lou, Y.; Liu, J. CO Oxidation on Metal Oxide Supported Single Pt Atoms: The Role of the Support. *Ind. Eng. Chem. Res.* **2017**, *56* (24), 6916–6925. https://doi.org/10.1021/acs.iecr.7b01477.

(46) Lin, J.; Chen, Y.; Zhou, Y.; Lin, L.; Qiao, B.; Wang, A.; Liu, J.; Wang, X.; Zhang, T. More Active Ir Subnanometer Clusters than Single-Atoms for Catalytic Oxidation of CO at Low Temperature. *AIChE J.* **2017**, *63*, 4003–4012. https://doi.org/10.1002/aic.15756.

(47) Jentys, A. Estimation of Mean Size and Shape of Small Metal Particles by EXAFS. *Phys. Chem. Chem. Phys.* **1999**, *1* (17), 4059–4063. https://doi.org/10.1039/A904654B.

(48) Alexeev, O. S.; Chin, S. Y.; Engelhard, M. H.; Ortiz-Soto, L.; Amiridis, M. D. Effects of Reduction Temperature and Metal−Support Interactions on the Catalytic Activity of Pt/γ-Al_2O_3 and Pt/TiO_2 for the Oxidation of CO in the Presence and Absence of H_2. *J. Phys. Chem. B* **2005**, *109* (49), 23430–23443. https://doi.org/10.1021/jp054888v.

(49) Engel, T.; Ertl, G. Elementary Steps in the Catalytic Oxidation of Carbon Monoxide on Platinum Metals. *Adv. Catal.* **1979**, *28*, 1–78.

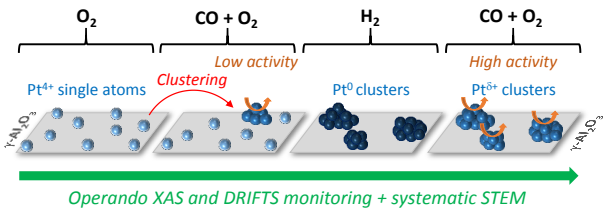
O2
CO + O2
H2
CO + O2
Low activity
High activity
Clustering
Pt4+ single atoms
Pt0 clusters
Pt5+ clusters
γ-Al2O3
γ-Al2O3
Operando XAS and DRIFTS monitoring + systematic STEM